Journal of Electronic Materials (2021) 50:4450–4455
https://doi.org/10.1007/s11664-021-08980-y

ORIGINAL RESEARCH ARTICLE

Effect of KrF Laser Irradiation on the Morphology and Microstructure of Amorphous PZT Thin Films Grown by RF Magnetron Sputtering

Mohammed Mahdi[1,2] · Mohamed Kadri[1]

Received: 22 November 2020 / Accepted: 24 April 2021 / Published online: 14 May 2021
© The Minerals, Metals & Materials Society 2021

Abstract

This work deals with the crystallization of amorphous PZT thin films, induced by a 248 nm KrF laser source. PZT thin films, 250 nm thick, were grown on three different substrates (Si/SiO_2/Ti/Pt, Si/SiO_2, and glass/Al) using radio-frequency magnetron sputtering. The films were then treated with laser beams with energy density from 10 mJ/cm^2 to 100 mJ/cm^2. The morphology of the films was investigated by scanning electron microscopy (SEM) and the surface roughness by atomic force microscopy (AFM). The microstructure was evaluated using x-ray diffraction (XRD) and ellipsometry. The formation of square wells with 10 µm sides was detected on the surface of the Si/SiO_2/Ti/Pt/PZT samples. However, the measured roughness was 11 nm. Microstructure analysis showed good crystallization with dominant orientation of (110) and grain size of 229.6 nm at 30 mJ/cm^2, 25 mJ/cm^2 and 20 mJ/cm^2. For Si/SiO_2/PZT samples, the surface morphology was seriously deteriorated. Microstructure analysis revealed a weak (110) reflex with grain size of 110 nm at 20 mJ/cm^2. However, ablation began at 25 mJ/cm^2, and at lower energy densities of 10 mJ/cm^2 and 15 mJ/cm^2, the presence of only a pyrochlore phase was observed. For the glass/Al/PZT sample, ablation occurred at 15 mJ/cm^2, and microstructure analysis showed an amorphous phase at 10 mJ/cm^2.

Keywords PZT · thin films · RF magnetron sputtering · KrF laser · crystallization

Introduction

The integration of new functional materials in semiconductor technology opens new doors for a wide range of applications.[1] Ferroelectric and piezoelectric ceramics such as PZT have been studied intensively for microelectromechanical systems (MEMS) and ferroelectric random access memory (FeRAM),[2] tomography[3] and humidity sensing.[4] However, their application in integrated circuit (IC) technology[5] or sensitive temperature substrates is quite difficult, mainly regarding their high-temperature processing[6]. In order to overcome the issues with conventional thermal treatment,[7] laser technology seems to be an excellent candidate,[8–10] delivering enough energy in a short time and selective area for high-temperature processing.[11]

Many studies on laser crystallization have been performed using different kinds of light sources.

Bharadwaja et al. used an excimer laser with 248 nm wavelength delivering 4.99 eV of energy, which is larger than the PZT band gap (3.5 eV), directly on the surface of the films, creating homo-nucleation around defects on the top of the amorphous PZT thin films.[12]

Chou et al.[13] used a CO_2 laser with 10.6 µm wavelength absorbed by aluminum under-layer metallization and substrate, leading to hetero-nucleation of PZT from the substrate, and the results showed that the remnant polarization was sevenfold higher than that reached by the KrF laser. Similarly, Elshin et al.[14] used multiple pulses of a near-infrared femtosecond laser in the absorption region of a platinum under-layer. This laser is more specific for any IC integration, and the results showed explosive crystallization at the interface.

In our work, PZT thin films 250 nm in thickness were directly exposed to 248 nm laser irradiation. The material

✉ Mohammed Mahdi
mmahdi@cdta.dz

1 LMESM, Oran University of Science and Technology - Mohamed Boudiaf USTOMB, El Mnaouar, BP 1505, Bir El Djir, Oran, Algeria

2 MEMS & Sensors, Division Microélectronique et Nanotechnologie, Centre de Développement des Technologies Avancées (CDTA), BP 17, Baba Hassen, Algiers, Algeria

completely absorbed the energy delivered by the source. Different substrates were employed ($Si/SiO_2/Ti/Pt$, Si/SiO_2, and glass/Al substrates) in order to show the influence of the under-layer on the film crystallization.

Experimental Setup

Amorphous PZT Thin Film Growth

[$Si/SiO_2/Ti/Pt$], [Si/SiO_2] and [glass/Al] substrates were used in the experiment. The homemade target of $Pb(Zr_{0.5}, Ti_{0.5})$ was applied in a radio-frequency (RF) magnetron sputtering system,[15–17] and the main parameters are listed in Table I. Sputtering deposition at room temperature led to the growth of amorphous thin films on all substrates.

Laser Treatment of the Amorphous PZT Surface

A pulsed excimer KrF laser with emission at 248 nm was used to irradiate the thin film surfaces. Laser pulses of 20 ns, 10 Hz frequency and rectangular (1×2 cm^2) spot shape were used. The treatment was conducted under an ambient environment at room temperature. The main parameters are summarized in Table II.

Table I RF magnetron sputtering parameters for PZT thin film growth.

Target	Homemade target of $Pb(Zr_{0.48} Ti_{0.52})O_3$
Target diameter	7.6 cm
Target substrate distance	5 cm
RF power on target	150 W
Sputtering gas	Argon
Sputtering pressure	2 Pa
Sputtering time	120 min
In situ annealing	Room temperature

Morphology and Surface Investigation

The cross section of the thin films was observed using a Philips XL30-FEG scanning electronic microscope (SEM) under electron energy of 20 kV. We used a JEOL JSM 6360LV instrument to investigate the surface morphology at the same electron energy. Atomic force microscopy (AFM; JEOL 5200) was applied to determine the surface roughness.

Microstructure and Crystallization

The x-ray diffraction (XRD) patterns were recorded using a Bruker D8 Advance diffractometer equipped with a CuKα radiation source (λCuKα=1.5406 Å) operated at 40 kV and 40 mA. A grazing incidence configuration was used for analysis of the thin films, with a 2θ range of 15° to 80° and 10° path.

Results and Discussion

In Table II, we note naked-eye observations during laser treatment for each sample.

Morphology and Surface Roughness

We observe that ablation occurs on the PZT thin films deposited on glass substrate metalized with aluminum even at low energy of 10 mJ/cm^2 (see Table II).

In the samples based on Si/SiO_2 substrates, dramatic destruction of the thin film surface is observed by the naked eye (see Table II) at low energy density of 15 mJ/cm^2, and ablation appears at 25 mJ/cm^2.

However, in the samples based on $Si/SiO_2/Ti/Pt$ substrates, ablation occurred only at 40 mJ/cm^2, and the samples absorbed the energy from 10 mJ/cm^2 to 30 mJ/cm^2 (Fig. 2) without macroscopic damage to the thin film surface. The SEM images of the samples are shown in Figs. 1 and 2.

In Fig. 1, the thin film is measured by tilting the substrate, and the cross section indicates average film thickness of 250 nm.

Table II Laser treatment parameters and observations during the experiment.

	Observation by the naked eye during the experience		
	$Si/SiO_2/Ti/Pt/PZT$ 1000 pulses	Glass/Al/PZT 10 pulses then 100 pulses	$Si/SiO_2/PZT$ 1000 pulses
10 mJ/cm^2	Nothing to report	Some ablation of PZT	Nothing to report
15 mJ/cm^2	Nothing to report	Total ablation of PZT	Color change/dull color
20 mJ/cm^2	Nothing to report	Total ablation of PZT	Color change/dull color
25 mJ/cm^2	Nothing to report	Total ablation of PZT	Some ablation/dull color
30 mJ/cm^2	Some evaporation	Total ablation of PZT	Ablation/dull color

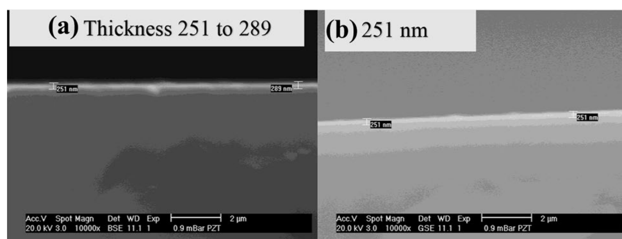

Fig. 1 Tilted substrate showing cross section using (a) BSE detector and (b) GSE detector. The PZT thin film thickness is estimated to be 250 nm.

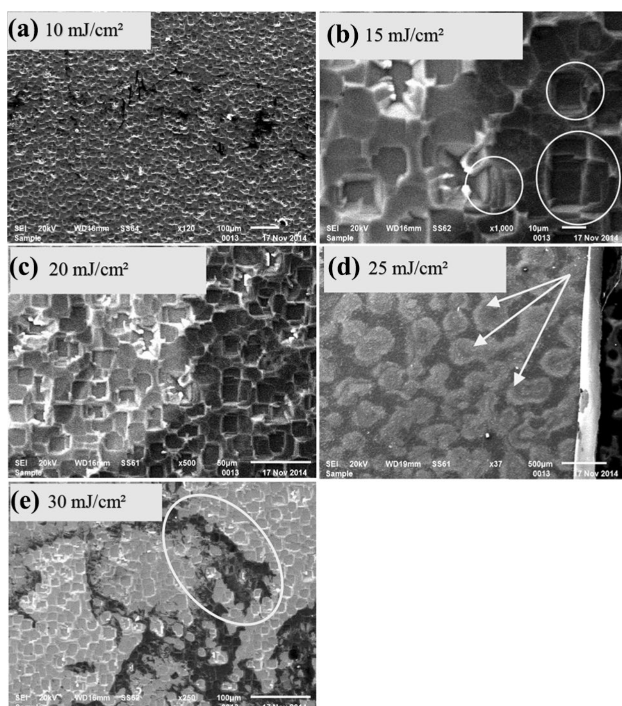

Fig. 2 Surface morphology of the PZT thin films deposited on Pt/Ti/SiO_2/Si substrates. (a) Surface morphology at 10 mJ/cm^2, (b) 15 mJ/cm^2 the square well of 10 µm size, (c) 20 mJ/cm^2 surface damage induces by the laser, (d) 25 mJ/cm^2 the nucleation of the perovskite phase induced by the laser energy, (e) ablation of the thin films of PZT.

In Fig. 2, the surface morphology after laser treatments for samples based on Si/SiO_2/Ti/Pt are presented. The formation of square wells is observed on the surface, caused by the ablation of the material under laser irradiation at 10 mJ/cm^2, 15 mJ/cm^2 and 20 mJ/cm^2 and square wells of 10 µm in size are observed. In the image of the relief formed at 25 mJ/cm^2, we observe nucleation islands of the perovskite corresponding to the PZT structure, and similar results are reported by Refs.[15, 17–20].

At 30 mJ/cm^2, we observe degradation of the thin films due to the ablation of the material.

The surface roughness was clearly affected by the laser treatment. The 2D SPM images are shown in Fig. 3 for the surface treated at 30 mJ/cm^2 and 25 mJ/cm^2. The roughness measured is 11.8 and 13 nm, respectively. However, when the as-deposited PZT thin films are annealed at 600°C for 1 h, the surface roughness measured on the 3D AFM imaging is 44 nm.

X-ray Diffraction (XRD) Analysis and Ellipsometry

The x-ray diffraction (XRD) patterns of the PZT/Pt/Ti/SiO_2/Si samples treated at 30 mJ/cm^2, 25 mJ/cm^2 and 20 mJ/cm^2 reveal the formation of a perovskite-type structure by the appearance of (001) (100) (110) and (200) reflexes. The (110) reflex is of the highest relative intensity, and the grain size estimated by the peak is as high as 229.6 nm, which is almost the whole thickness of the PZT thin film. Comparing these finding with Ref. 15, we could say that almost 20 nm of thickness remained amorphous in the interface between the under-layer and the PZT thin films (Fig. 4).

The XRD patterns for the films on glass and Si/SiO_2 substrates are shown in Fig. 5. Despite the significant damage on the surface after laser treatments, the microstructure on Z3 shows the formation of a weak peak at 2θ equal to 30.61° where the plane (110) is located with a grain size of 108 nm, at 20 mJ/cm^2. However, at 15 and 10 mJ/cm^2 on Z2 and Z1 respectively, the pyrochlore phase ($A_2B_2O_7$) is obtained. Finally, the only case in which an amorphous phase is obtained is when a glass substrate is used.

An amorphous film was formed on the glass/Al substrate. We used the model reported previously in Refs.[21–23], which is based on the Forouhi-Bloomer model (Eqs. 1 and 2).

$$n(E) = n(\infty) + \frac{BE + C}{E^2 - BE + C} \tag{1}$$

$$K(E) = \frac{A(D - E)}{E^2 - BE + C} \tag{2}$$

We obtain a double peak near 3.4 eV (400 nm) and 4.2 eV (300 nm) energy Fig. 6. Comparing these results with Lee et al.[24] work, we conclude that the pyrochlore phase is dominant, and is located near 4 eV energy. However, the small perovskite phase is around 3 eV.

The parameters $A = 0.078$, $B = 10.82$, $C = 30.87$, $E_g = 2.99$ were taken from the study by Yang et al.[25] for amorphous PZT. Our fit on the amorphous zone shows that we have 50 nm thickness with parameters $A = 0.7$, $B = 5.8$, $C = 12.9$, $E_g = 2.7$. These results confirm the XRD analysis.

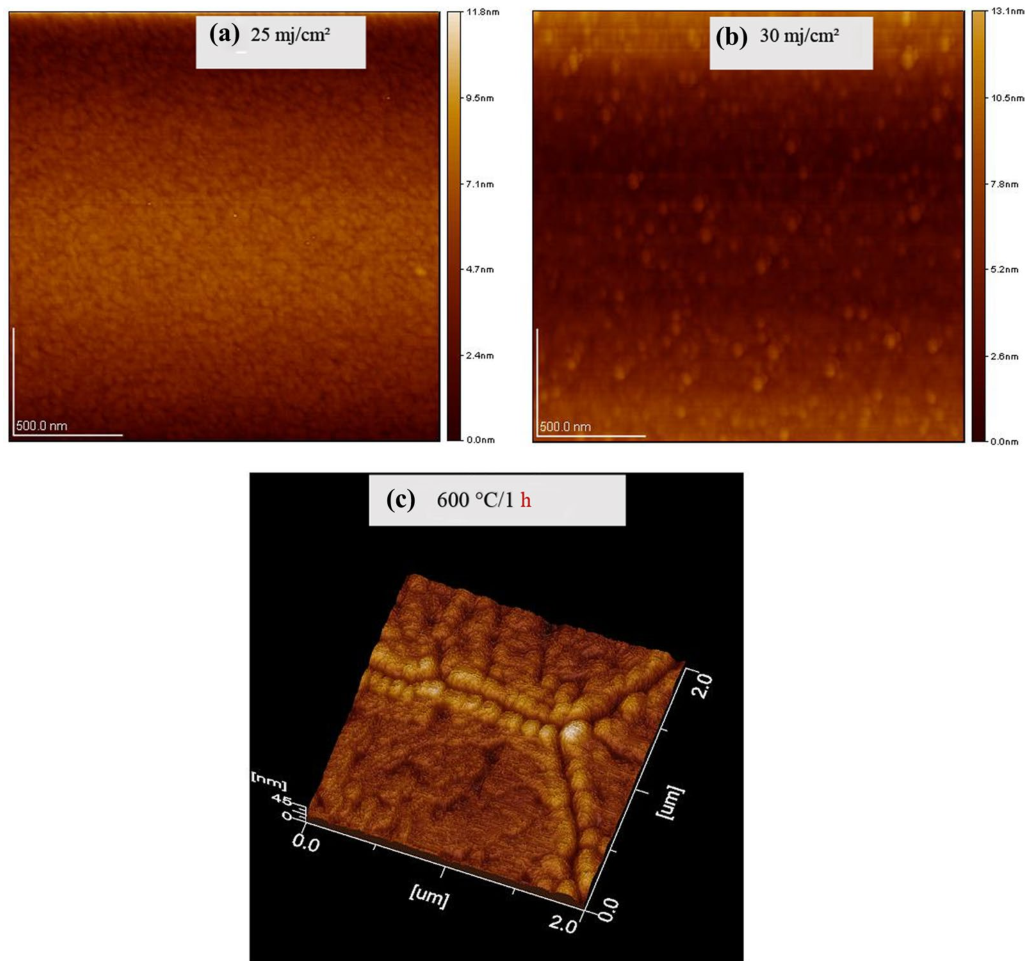

Fig. 3 Atomic force microscopy (AFM) on $PZT/Pt/Ti/SiO_2/Si$ surfaces showing roughness of (a) 11.8 nm for 30 mJ/cm^2 and (b) 13 nm for 25 mJ/cm^2. (c) 3D AFM showing roughness of 44 nm when the sample was annealed at 600°C for 1 h.

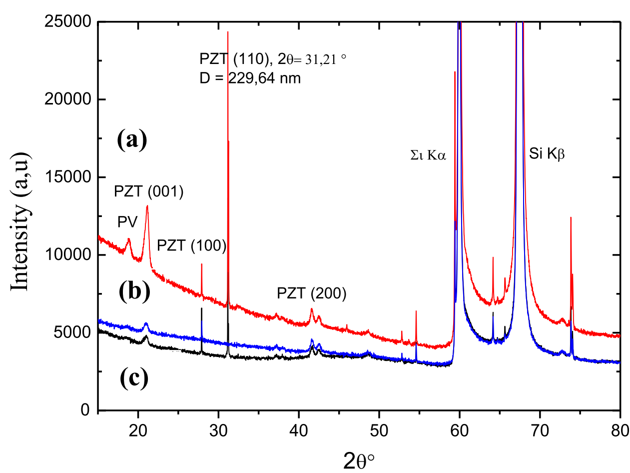

Fig. 4 XRD patterns of the PZT thin films onto $Pt/Ti/SiO_2/Si$ substrate. The film is irradiated at (a) 30 mJ/cm^2, (b) 25 mJ/cm^2 and (c) 20 mJ/cm^2.

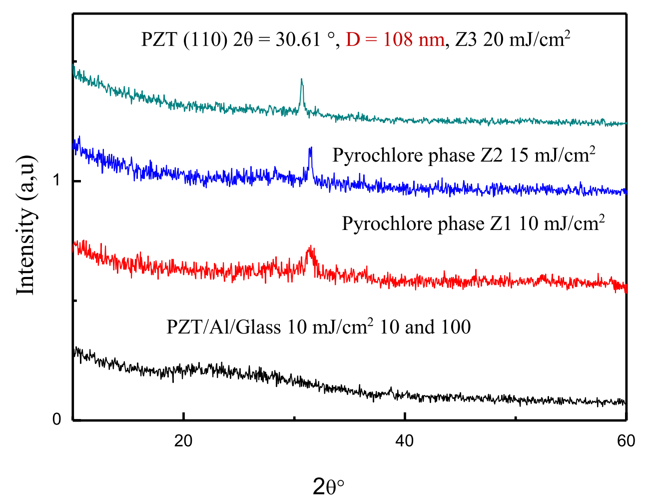

Fig. 5 XRD patterns for the PZT thin films deposited on SiO_2/Si substrate and glass/Al substrate.

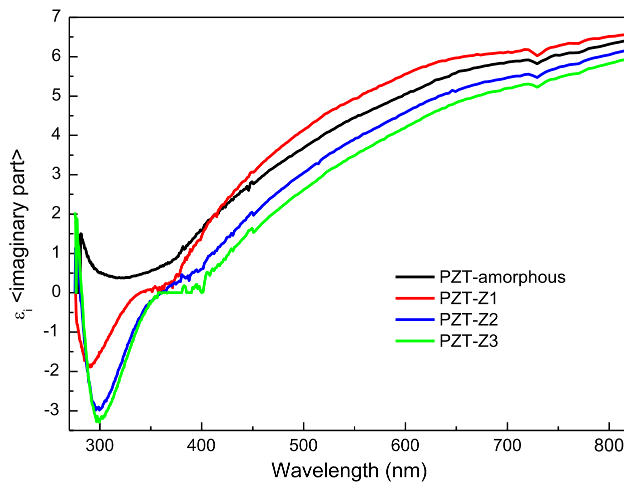

Fig. 6 Dispersive imaginary part of dielectric function as a function of photon energy for the PZT thin films deposited on glass and SiO_2/Si substrate, Z1 for 10 mJ/cm^2, Z2—15 mJ/cm^2 and Z3—20 mJ/cm^2.

Conclusion

In this work, we demonstrate that the crystallization of amorphous PZT film can be induced by KrF 248 nm laser top treatment. The optimum crystallization conditions for silicon substrate with the conventional (Ti/Pt) under-layer usually used for PZT thin films is around 15–20 mJ/cm^2 energy density.

The combination with conventional bottom heat treatment at 400°C (which is the maximum temperature for which IC chips are authorized) and laser top irradiation is the perfect process adapted for MEMS-compatible CMOS technology solutions, compared with the most recent advances by ULVAC[26] in the development of new reactor configurations aimed at the growth of crystallized PZT thin films at 500°C to achieve CMOS compatibility.

Nevertheless, the dielectric, ferroelectric, and piezoelectric properties are related to the microstructure and not to the morphology of the thin films. The surface topography obtained after laser treatment has many effects on the mechanical and physical properties, which could be investigated in depth elsewhere. For instance, many pyroelectric applications seek a similar surface morphology by many process steps in order to trap the maximum light.[27]

On the other hand, laser treatment significantly reduces the roughness of the surface due to the partial melting of the top of the thin films compared with conventional heat treatment, which enhances the mechanical properties for MEMS applications.

Acknowledgments The authors thank Dr. Y. Jeridan and Dr. S. Lafane for their technical support for this work.

Funding This work was supported by "Laboratoire de Microscopie Electronique & Sciences des Matériaux" and MEMS & Sensors team at CDTA.

Conflict of interest The authors declare that they have no conflict of interest.

References

1. J. Zhu, X. Liu, Q. Shi, T. He, Z. Sun, X. Guo, W. Liu, O.B. Sulaiman, B. Dong, and C. Lee, *Micromachines* 11, 7 (2019). https://doi.org/10.3390/mi11010007.
2. H. Ishiwara, Recent progress in ferroelectirc memory technology, in *Proc. 8th Int. Conf. Solid-State Integr. Circuit Technol.* (2006), pp. 713–716. https://doi.org/https://doi.org/10.1109/ICSICT.2006.306466.
3. S. Wang, W. Wu, Y. Shen, Y. Liu, and S. Jiang, *Sensors* 20, 860 (2020). https://doi.org/10.3390/s20030860.
4. H.A. Gatea, I. Naji, and A. Abulameer, *Int. J. Thin Film Sci. Technol.* 9, 143 (2020). https://doi.org/10.18576/ijtfst/090208.
5. I. Bretos, R. Jiménez, and M. Tomczyk, *Sci. Rep.* 6, 20143 (2016). https://doi.org/10.1038/srep20143.
6. P.P. Donohue, M.A. Todd, and Z. Huang, *Integr. Ferroelectr.* 51, 39 (2003). https://doi.org/10.1080/10584580390229770.
7. T. Miyazaki, T. Imai, N. Wakiya, N. Sakamoto, D. Fu, and H. Suzuki, *Mater. Sci. Eng. B* 173, 89 (2010). https://doi.org/10.1016/jmseb200912017.
8. S.S.N. Bharadwaja, T. Dechakupt, S. Trolier-MacKinstry, and H. Beratan, *J. Am. Ceram. Soc.* 91, 1580 (2008). https://doi.org/10.1111/j.1551-2916.2008.02313.x.
9. A. Elshin, N. Firsova, M. Marchenkova, V. Emel'yanov, I. Pronin, S. Senkevich, E. Mishina, and A. Sigov, *Tech. Phys. Lett* 41, 418 (2015). https://doi.org/10.1134/S1063785015050041.
10. X.M. Lu, J.S. Zhu, W.S. Hu, Z.G. Liu, and Y.N. Wang, *Appl. Phys. Lett.* 66, 2481 (1995). https://doi.org/10.1063/1.114002.
11. A.S. Elshin, N.Y. Firsova, M.A. Marchenkova et al., *Tech. Phys. Lett.* 41, 418 (2015). https://doi.org/10.1134/S1063785015050041.
12. S.S.N. Bharadwaja, F. Griggio, J. Kulik, and S. Trolier-McKinstry, *Appl. Phys. Lett.* 99, 042903 (2011). https://doi.org/10.1063/1.3615295.
13. C.F. Chou, H.C. Pan, and C.C. Chou, *Jpn. J. Appl. Phys.* 41, 6679 (2002). https://doi.org/10.1143/JJAP.41.6679.
14. A. Elshin, N. Firsova, V. Emelianov, I. Pronin, S. Senkevich, O. Zhigalina, E. Mishina, and A. Sigov, *J. Phys. Conf. Ser* 661, 012037 (2015). https://doi.org/10.1088/1742-6596/661/1/012037.
15. D.N. Khmelenin, O.M. Zhigalina, K.A. Vorotilov et al., *Phys. Solid State* 54, 999 (2012). https://doi.org/10.1134/S1063783412050174.
16. M. Mahdi, and M. Kadri, *DDF* 406, 256 (2021). https://doi.org/10.4028/www.scientific.net/ddf.406.256.
17. M. Mahdi, and M. Kadri, *Appl. Mech. Mater.* 464, 89 (2014). https://doi.org/10.4028/www.scientific.net/amm.464.89.
18. I.P. Pronin, EYu. Kaptelov, S.V. Senkevich, V.A. Klimov, N.V. Zaitseva, T.A. Shaplygina, and S.A. Kuku-shkin, *Phys. Solid State* 52, 132 (2010). https://doi.org/10.1134/S1063783410010233.
19. I.Y. Tentilova, E.Y. Kaptelov, I.P.I. Pronin, and V.L. Ugolkov, *Inorg. Mater.* 48, 1136 (2012). https://doi.org/10.1134/S0020168512110155.
20. S.A. Kukushkin, I.Y. Tentilova, and I.P. Pronin, *Phys. Solid State* 54, 611 (2012). https://doi.org/10.1134/S1063783412030158.
21. V.N. Kruchinin, T.V. Perevalov, and V.V. Atuchin, *J. Electron. Mater.* 46, 6089 (2017). https://doi.org/10.1007/s11664-017-5552-3.

22. V.V. Atuchin, M.S. Lebedev, I.V. Korolkov et al., *J. Mater. Sci. Mater. Electron.* 30, 812 (2019). https://doi.org/10.1007/s10854-018-0351-z.
23. C.V. Ramana, V.H. Mudavakkat, K. Kamala Bharathi, V.V. Atuchin, L.D. Pokrovsky, and V.N. Kruchinin, *Appl. Phys. Lett.* 98, 031905 (2011). https://doi.org/10.1063/1.3524202.
24. H. Lee, Y. Kang, S. Cho, B. Xiao, H. Morkoç, T. Kang, G. Lee, J. Li, S. Wei, P. Snyder, and J. Evans, *J. Appl. Phys.* 98, 094108 (2005). https://doi.org/10.1063/1.2128043.
25. S. Yang, D. Mo, and X. Tang, *J. Mater. Sci.* 37, 3841 (2002). https://doi.org/10.1023/A:1019682817298.
26. H. Kobayashi, Thin-film processing technologies of piezoelectric materials for IoT/IoE applications, in *2020 IEEE 33Rd International Conference on Micro Electro Mechanical Systems (MEMS)* (IEEE, 2020), pp. 550–553. https://doi.org/10.1109/MEMS46641.2020.9056215.
27. C. Hsiao, J. Ciou, A. Siao, and C. Lee, *Sensors* 11, 11 (2011). https://doi.org/10.3390/s111110458.

Publisher's Note Springer Nature remains neutral with regard to jurisdictional claims in published maps and institutional affiliations.